Routing and Spectrum Allocation in Broadband Degenerate EPR-Pair Distribution

Rohan Bali*, Ashley Tittelbaugh*, Shelbi L. Jenkins*, Anuj Agrawal†
Jerry Horgan‡, Marco Ruffini†, Daniel Kilper‡, Boulat A. Bash*
*Electrical and Computer Engineering Department, University of Arizona, Tucson, AZ, USA
†School of Computer Science and Statistics, CONNECT Centre, Trinity College Dublin, Dublin, Ireland
‡Electronic and Electrical Engineering Department, CONNECT Centre, Trinity College Dublin, Dublin, Ireland

***Abstract*—We investigate resource allocation for quantum entanglement distribution over an optical network. We characterize and model a network architecture that employs a single quasi-deterministic time-frequency heralded EPR-pair source, and develop a routing scheme for distributing entangled photon pairs over such a network. We focus on max-min fairness in entanglement distribution and compare the performance of various spectrum allocation schemes by examining both the max-min number of EPR pairs assigned by them and the Jain index associated with this assignment.**

I. Introduction

Quantum entanglement distribution over a network is essential for large-scale quantum computing, quantum sensing, and quantum security. Although various protocols have been proposed [1], the entanglement *source-in-the-middle* approach is efficient in many practical settings. A promising source-in-the-middle method employs a broadband degenerate quasi-deterministic time-frequency heralded Einstein-Podolsky-Rosen (EPR) pair source [2]. Wavelength-selective routing can then be used to distribute the broadband entangled-photon pairs to consumer node pairs in a network.

The scheme from [2] has the advantage of producing EPR pairs that are heralded in time and frequency, however, it presents unique challenges in routing and spectrum allocation. The source in [2] is degenerate: it outputs entangled photon pairs on the same wavelength. Thus, photons from a given pair cannot use the same fiber span in the same direction without routing ambiguity or requiring time multiplexing. Routing algorithms must account for this, along with path-dependent photon losses. Furthermore, although the source is broadband, when segmented into narrow-band channels, the average number of entangled photon pairs it generates per channel varies across the spectrum. Here, we build upon the classical approaches [3] to develop routing and spectrum allocation strategies for single-source entanglement distribution.

Fortunately, in our single-source setting, routing and spectrum allocation can be addressed separately. We adapt Suurballe's algorithm [4], [5] to find an optimal route in polynomial time. We desire max-min fair spectrum allocation, where the minimum number of EPR pairs each node receives is maximized. Unfortunately, as in classical optical networks [6], this is an NP-hard integer linear program (ILP). Therefore, we investigate the performance of various approximation algorithms, and compare them to the optimal ILP solution on a small toy network. We also address the source placement problem, i.e., finding the optimal location for our entangled photon source. Thus, we analyze both the fairness with which different algorithms can supply heralded EPR pairs throughout the network and the properties of the ideal locations of the source node.

Previous works have achieved entanglement distribution by placing an EPR pair source at each node in a point-to-point (PTP) network that uses wavelength-division multiplexers (WDMs) [7]. However, this necessitates physical connections between each pair of nodes, as well as EPR pair sources at each node, both of which present scaling challenges. A fully passive approach with WDMs was used to distribute EPR pairs across a four-node network in a single-source setting [8]. This was extended to allow for adaptive spectrum allocation in quantum networks: [9] uses a wavelength selective switch (WSS) and [10] uses a re-configurable optical add-drop multiplexer (ROADM) to distribute spectrally-correlatedpolarization-entangled photon pairs. By using hyper-entangled states in polarization and frequency along with quantum-enabled ROADMs, [11] demonstrated active switching to allocate channels of different bandwidths to different nodes, and also to demultiplex the channels at the nodes. However, these works do not address the problem of routing photons in a large network. On the other hand, the degenerate approach [2] used here has not been realized in experiments nor studied from a wavelength-routing perspective.

Section II overviews the source and network architectures and their models. Section III discusses our approaches for optimizing routing and spectrum allocation. Section IV compares our approaches numerically. We discuss the implications of our results and future work in Section V.

II. System Model

A. Broadband Degenerate EPR-pair Generation

We assume the availability of a broadband, quasi-deterministic EPR-pair source. An example of such is the zero-added loss entangled multiplexing (ZALM) scheme described

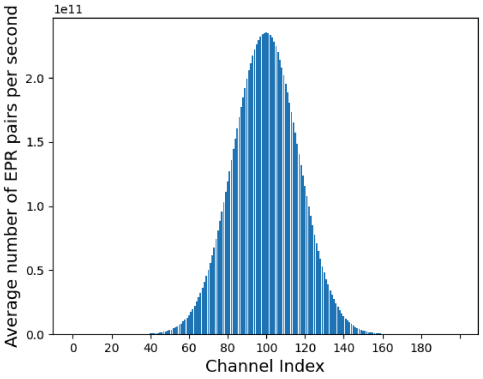

Fig. 1. Rate of EPR pair generation in 200 channels.

in [2]. It employs dual spontaneous parametric down-conversion (SPDC) processes. This source heralds entangled photon pairs by wavelength demultiplexing the broadband spectrum and detecting coincidence counts occurring at the same wavelength for two idler photons each generated by individual SPDC processes. The corresponding heralded signal photons of now known and identical wavelength are directed through a WDM system with wavelength-selective add-drop capability.

Each SPDC source produces entangled photons at the rate that follows a Gaussian function that we assume is centered at 1550 nm with a full-width half max of 9 nm. As depicted in Fig. 1, the spectrum is segmented into $m = 200$ channels, each covering a 0.1 nm wavelength range. The central channel is positioned at the peak of the Gaussian distribution. Thus, the lowest and highest indexed channels correspond to a center frequencies of 195.9 THz and 191.1 THz with bandwidths of 12.8 GHz and 12.2 GHz, respectively. WDM prior to Bell measurement enables heralding of the generated EPR pair's channel index. The channels are spaced 0.1 nm apart to prevent fidelity loss from wavelength ambiguity. Due to the Gaussian relationship, the average EPR pair generation rate per second for channels near 1550 nm is higher than for those on the edges of the spectrum. The ZALM source is depicted in Fig. 2(a) as 'Source Node A.' Note that our analysis that follows can be adapted to other methods of generating degenerate EPR pairs. The output spectrum from this source can be routed and distributed across the network using WDM routing techniques like those that have been developed for classical optical networks [3].

B. Node Architecture

Each photon of the generated EPR pair is directed by the source into a separate fiber. The node is built around $1 \times N$ WSSs, whose role is to route wavebands towards different consumer nodes or else towards its own quantum memory bank. These wavebands group the source wavelength channels depicted in Fig. 1. Information heralded by the EPR pair generation process (including the channel and timestamp of the generated pair) is transmitted along a classical network that is not depicted here. A consumer node lacks EPR pair generation capability, but has all the other components of the source node. The block diagrams for both the source and consumer nodes are in Fig. 2(a).

Measured insertion loss l_{WSS} on Lumentum's TrueFlex Twin WSS ranges from 4 dB to 8 dB [12]. Hence we analyze EPR pair distribution for two values of WSS loss: $l_{\text{WSS}} \in \{4, 8\}$ dB. While they add significant loss, we note that WSSs are currently manufactured for use in classical networks and, thus, are not optimized for loss reduction. Other wavelength management and switching devices can achieve a loss of 2 dB [13]. Here we assume wavelength-independent loss l in dB that is related to power transmittance by $\eta = 10^{-l/10}$.

C. Network Topologies

Our main topology model is an existing incumbent local exchange carrier (ILEC) node map of Manhattan [14], [15]. This topology contains $n = 17$ ILEC sites, with each site connected to between 2 and 16 other nodes. The layout of these nodes is shown in Fig. 3. While this is the reference topology for validating the performance of our heuristics, the comparison with an optimal ILP solution is restricted to a smaller network topology with $n = 6$ nodes, shown in Fig. 4, because the optimal fair allocation of EPR pairs is an NP-hard problem.

D. Network Architecture

The deployed fiber link lengths between nodes in the ILEC topology depicted in Fig. 3 are unknown. Thus, we use direct 'as the crow flies' distance as a proxy. Standard single-mode fiber is assumed on each link. We employ a higher loss coefficient of $\alpha = 0.4$ dB/km than typical fiber loss at 1550 nm (found in, e.g., [16]) to account for higher losses and longer run lengths characteristic of metro fiber plant. We assume that all pairs of nodes in the network request EPR pairs from the source. Each wavelength channel is assigned to a single pair. The wavelength routing mechanism follows a circuit-switching approach. The routes serving different sets of node pairs do not interfere with one another, however, photons from a particular channel cannot be directed to two different nodes of a pair via the same fiber in the same direction, as this results in a routing ambiguity. Therefore, we only consider networks that allow disjoint light-paths from the source to each of the k pairs of consumer nodes.

E. Network Model

We represent a network as a graph denoted by $\mathcal{G} = (\mathcal{V}, \mathcal{E})$, where $\mathcal{V}$ and $\mathcal{E}$ are the sets of vertices and directed edges, respectively. We also define a map $w : \mathcal{E} \to \mathbb{R}$ that assigns photon losses (in dB) as edge weights. We construct $\mathcal{G}$ for the network topologies described in Section II-C as follows:

- For each pair (i, j) of connected consumer nodes we add the following directed edges and the corresponding vertices: $e_{j,\text{in}_i}^{i,\text{out}_j} \equiv \left(v_{i,\text{out}_j}, v_{j,\text{in}_i}\right)$ and $e_{i,\text{in}_j}^{j,\text{out}_i} \equiv \left(v_{j,\text{out}_i}, v_{i,\text{in}_j}\right)$ to $\mathcal{G}$. Hence each vertex is indexed by the node it belongs

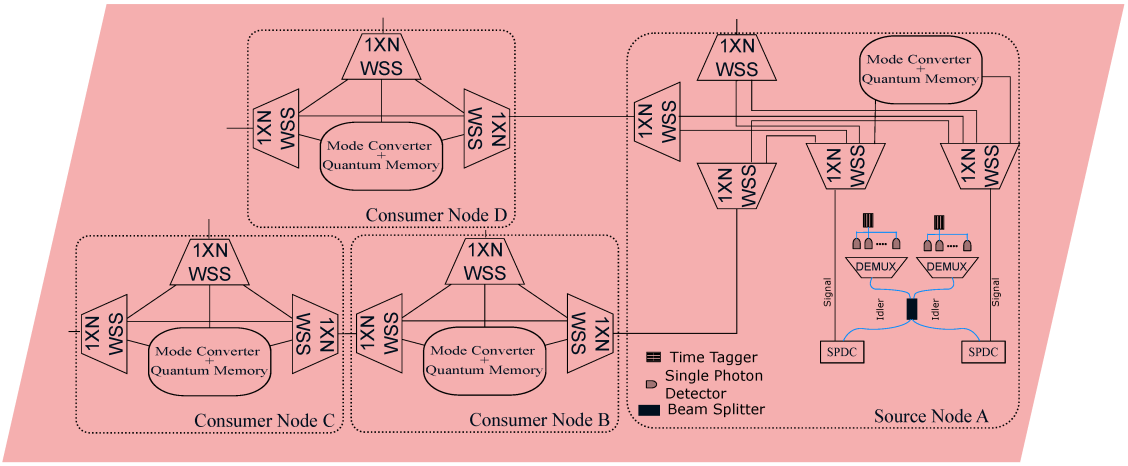

(a) Network Layout

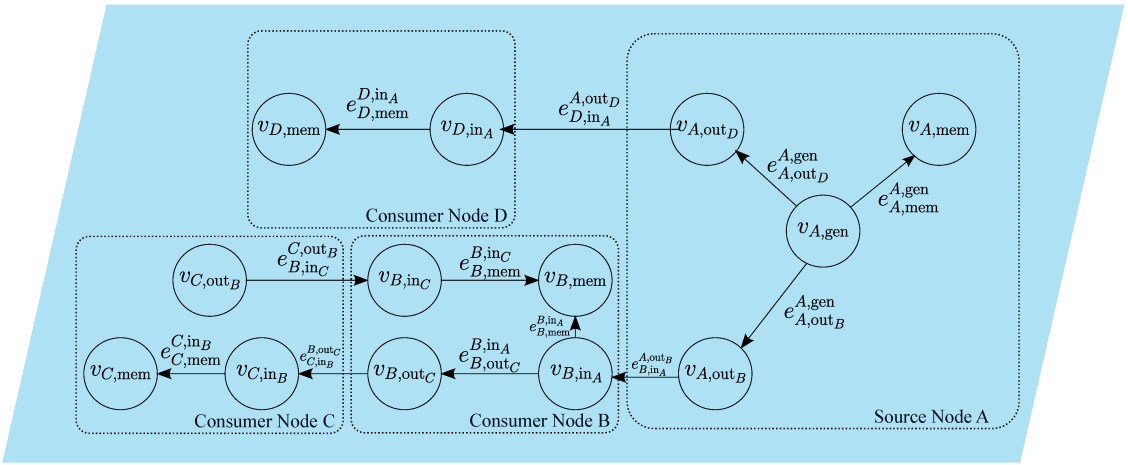

(b) Graph Model

Fig. 2. Correspondence between a network layout and its graph model. 2(a) shows a network of source (A) and consumer nodes (B, C, and D). 2(b) shows the corresponding graph model.

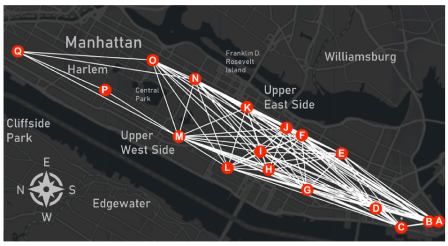

Fig. 3. A map of Manhattan with ILEC nodes and links overlaid.

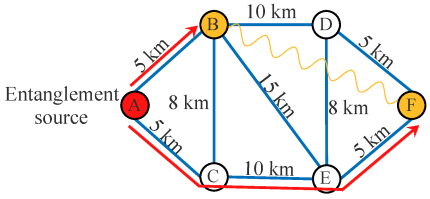

Fig. 4. Topology of the simple network.

to, and by the role of that vertex. Vertices that serve input/output roles have the name of the corresponding external node as a subscript. The weight of the edges is $w\left(e^{i,\text{out}_j}_{j,\text{in}_i}\right) = w\left(e^{j,\text{out}_i}_{i,\text{in}_j}\right) = \alpha \times d(i,j)$, where $d(i,j)$ is the distance (in km) between nodes i and j, and α is optical fiber loss (in dB/km) discussed in Section II-D.

- For each consumer node i, we iterate over all nodes j, k that connect to i, and add edges $e^{i,\text{in}_j}_{i,\text{out}_k} \equiv \left(v_{i,\text{in}_j}, v_{i,\text{out}_k}\right)$ to $\mathcal{E}$. This captures the consumer nodes' internal connections between incoming and outgoing ports. Since the photons routed through a consumer node must traverse two WSSes, the weight of these edges is $w\left(e^{i,\text{in}_j}_{i,\text{out}_k}\right) = 2l_{\text{WSS}}$, as discussed in Section II-D. Furthermore, we also add edges $e^{i,\text{in}_j}_{i,\text{mem}} \equiv \left(v_{i,\text{in}_j}, v_{i,\text{mem}}\right)$ describing internal connections to node i's quantum memory to $\mathcal{E}$, and the corresponding

vertices to $\mathcal{V}$. Since only one WSS is traversed in this case, $w\left(e_{i,\text{mem}}^{i,\text{in}_j}\right) = l_{\text{WSS}}$.

- For the source node s, we iterate over all nodes j that connect to s, and add edges $e_{j,\text{in}_s}^{s,\text{out}_j} \equiv \left(v_{s,\text{out}_j}, v_{j,\text{in}_s}\right)$ to $\mathcal{E}$ and corresponding vertices to $\mathcal{V}$. The weight of these edges is $w\left(e_{j,\text{in}_s}^{s,\text{out}_j}\right) = \alpha \times d(s,j)$. Consumer node's incoming vertices v_{j,in_s} are connected to outgoing vertices and quantum memories as described above. Finally, we add edges $e_{s,\text{out}_j}^{s,\text{gen}} \equiv \left(v_{s,\text{gen}}, v_{s,\text{out}_j}\right)$ and $e_{s,\text{mem}}^{s,\text{gen}} \equiv \left(v_{s,\text{gen}}, v_{s,\text{mem}}\right)$ from vertex $v_{s,\text{gen}}$ describing EPR pair generator to all outgoing ports and vertex $v_{s,\text{mem}}$ describing source's own quantum memory. The weights for these edges are $w\left(e_{s,\text{out}_j}^{s,\text{gen}}\right) = 2l_{\text{WSS}}$ and $w\left(e_{s,\text{mem}}^{s,\text{gen}}\right) = l_{\text{WSS}}$, per above. Note that the source node does not have incoming ports.

The total loss on a path from source to a consumer node i is the sum of weights of the edges connecting $v_{s,\text{gen}}$ to $v_{i,\text{mem}}$. Fig. 2(b) depicts a graph model corresponding to the four-node network shown in Fig. 2(a).

F. Max-min (Egalitarian) Fairness

We seek max-min, or egalitarian, fairness, and maximize the minimum average rate of EPR pairs received by all $k = n(n-1)/2$ pairs (i,j) of n nodes [17]. Let $l_{(i,j)}$ be the total loss (in dB) from the source to nodes (i,j). That is, $l_{(i,j)}$ is the sum of losses on the disjoint paths from source to nodes i and j, per Section II-E. Then, transmittance $\eta_{(i,j)} = 10^{-l_{(i,j)}/10}$ is the fraction of the entangled photon pairs that are received by (i,j). Let $\mathcal{A}_{(i,j)}$ be the set of channels assigned to node pair (i,j). Since each channel cannot be assigned to more than one node pair, the set $\mathcal{P} = \left\{\mathcal{A}_{(i,j)} : i,j = 1,\ldots,n, i \neq j\right\}$ partitions the m available channels. Let $\bar{n}_x$ be the average rate of EPR pair generated in channel x. The average rate of EPR pairs received by node pair (i,j) is then $\bar{n}_{(i,j)} = \eta_{(i,j)} \sum_{x \in \mathcal{A}_{(i,j)}} \bar{n}_x$ and the max-min fair allocation involves the following optimization: $\max_{\mathcal{P}} \min_{(i,j)} \bar{n}_{(i,j)}$.

III. Algorithms

Orthogonality of sets $\mathcal{A}_{(i,j)}$ allows treating routing and spectrum allocation problems separately, as discussed next.

A. Optimal routing

Unlike standard networks, our source-in-the-middle entanglement distribution system described in Section II requires two disjoint light paths from source s to nodes i and j that minimize total loss $l_{(i,j)}$ for each pair (i,j) in the network. Per Section II-E, this translates to finding edge-disjoint routes in $\mathcal{G}$ from $v_{s,\text{gen}}$ to $v_{i,mem}$ and $v_{j,\text{mem}}$ minimizing the sum of weights of these paths. To this end, we use Suurballe's algorithm [4], [5] as follows: for each consumer pair (i,j) we add a dummy vertex $v_{(i,j),\text{d}}$ to $\mathcal{V}$ and dummy zero weighted edges: $e_{(i,j),\text{d}}^{i,\text{mem}} \equiv \left(v_{i,\text{mem}}, v_{(i,j),\text{d}}\right)$ and $e_{(i,j),\text{d}}^{j,\text{mem}} \equiv \left(v_{j,\text{mem}}, v_{(i,j),\text{d}}\right)$ to $\mathcal{E}$. Suurballe's algorithm yields two edge-disjoint paths of minimum total weight between $v_{s,\text{gen}}$ and $v_{(i,j),\text{d}}$. Removing dummy vertices and edges returns edge-disjoint paths of minimum total weight from $v_{s,\text{gen}}$ to $v_{i,mem}$ and $v_{j,\text{mem}}$ for all pairs (i,j). Suurballe's algorithm's run-time is polynomial in graph size.

B. Spectrum Allocation Strategies

Let X be an $m \times n(n-1)/2$ binary matrix with $X_{x,(i,j)} = 1$ if channel x is assigned to node pair (i,j) and zero otherwise (note that the pair (i,j) indexes columns of X). Formally, $X_{x,(i,j)} = \left\{1 \text{ if } x \in \mathcal{A}_{(i,j)}; 0 \text{ else}\right\}$. Also define an $n(n-1)/2 \times n(n-1)/2$ diagonal matrix Λ with transmittances $\eta_{(i,j)}^*$ of optimal routes (see Section III-A) from source to each (i,j) on the diagonal and a vector $N = [\bar{n}_1, \ldots, \bar{n}_m]$ of average EPR-pair-generation rates in each channel (see Section II-F). For some X, the average rate of EPR pairs received by (i,j) is $\bar{n}_{(i,j)} = [NX\Lambda]_{(i,j)}$, the $(i,j)^{\text{th}}$ entry of vector $NX\Lambda$.

Finding an optimal spectrum allocation matrix X is a well-known problem in optical networking [6]. Here we focus on maintaining max-min fairness in source-in-the-middle entanglement distribution.

1) Optimal Assignment: The following integer linear program (ILP) yields the optimal max-min fair solution T_{opt}:

$$\max_X T \text{ s.t. } \sum_{\substack{i,j=1 \\ i \neq j}}^{n} X_{x,(i,j)} = 1, \forall x = 1,\ldots,m \tag{1a}$$

$$[NX\Lambda]_{(i,j)} \geq T, \forall i,j = 1,\ldots,n, i \neq j, \tag{1b}$$

where constraint (1a) enforces that each channel is assigned only once and (1b) ensures that each node pair receives EPR pair rate of at least T.

The routing scheme in our scenario implicitly enforces wavelength contiguity constraints, as wavelengths cannot be switched at intermediate nodes. This contrasts classical optical networks, where optimal spectrum allocation has to explicitly enforce them. Additionally, unlike classical networks that allow fractional channel allocation, source-in-the-middle entanglement distribution requires discrete channel assignment to entangle two particular quantum memories. This necessitates solving an NP-hard ILP problem. Hence, we consider approximations.

2) First Fit [6]: We assign channels sequentially to a node pair. If EPR pair rate T is reached, then we repeat for the next node pair. We restart with a smaller T if channels are exhausted before all node pairs attain EPR pair rate T.

3) Round Robin [18]: The channels are assigned one at a time to randomly ordered node pairs in the descending order of generated ERP pair rate.

4) Random: Each request is assigned roughly the same number of channels at random.

5) Modified Longest Processing Time First (LPT) [19], [20]: This is a well-known machine scheduling algorithm. We modify it to greedily optimize for the max-min rather than min-max goal, akin to [21]: each channel is assigned to a node pair which maximizes the current minimum received EPR pair rate across the node pairs. While our experiments indicate that this

approach performs well, we have not derived any analytical performance guarantees.

6) $1/(m-k+1)$*-approximation [17]:* This iterative polynomial-time algorithm converges to a solution that is guaranteed to be within $1/(m-k+1)$ of the optimal max-min value, where, in our setting m is the number of channels and $k = n(n-1)/2$ is the number of node pairs. We make two modifications: 1) instead of always assigning one channel to each node pair in each round, we allow skipping a channel assignment; 2) in each round, we prefer the assignment which minimizes the total rate of EPR pair generation that is assigned. These are invoked as long as it does not impact the overall max-min value, hence they can only increase the minimum received EPR pair rate for all node pairs, all the while preserving the original approximation guarantee.

7) $\max(0, T_{f\text{-}opt} - \max_{(i,j),x} \eta_{(i,j)}\bar{n}_x)$*-assignment guarantee [17]:* The minimum average EPR pair rate received by a node pair guaranteed by this algorithm is limited by the maximum EPR pair rate any node pair can receive: $\max(0, T_{\text{f-opt}} - \max_{(i,j),x} \eta_{(i,j)}\bar{n}_x)$, where $T_{\text{f-opt}}$ is the optimal solution to the integer linear program in (1) relaxed to allow fractional channel assignments. This algorithm first solves a linear program to obtain a fractional channel assignment, and then resolves assignments to multiple requests.

IV. Results and Discussion

In Figs. 5(a) and 6(a) we report unnormalized and normalized minimum average received EPR pair rates for topologies described in Section II-C. Normalization is with respect to the highest-loss consumer pair's photon count across source node locations, when assigned all channels, i.e.: $\min_{(i,j)} \eta_{(i,j)} \sum_{x=1}^{m} \bar{n}_x$. In Figs. 5(b) and 6(b) we report the Jain index [22] $\frac{(\sum_{(i,j)} \bar{n}_{(i,j)})^2}{\frac{n(n-1)}{2} \sum_{(i,j)} \bar{n}^2_{(i,j)}}$, which ranges from 1 (completely fair) to $\frac{1}{n(n-1)/2}$ (most unfair). Results from random and $\max(0, T_{\text{f-opt}} - \max_{(i,j),x} \eta_{(i,j)}\bar{n}_x)$ algorithms are not reported for the Manhattan topology in Fig.6(a) as their performance is as poor as those shown in Fig. 5(a) for the simple network.

The first-fit and round-robin algorithms are sensitive to the node pair order. The random assignment can yield varying performance metrics across different executions. Also, although the ILP algorithm consistently produces the same minimum number of assigned average EPR pair rates in each run, it may use distinct assignment configurations, resulting in varying Jain index. Thus, the results for the first-fit, random, round-robin, and ILP algorithms are averaged over 1000 runs, with each run randomizing the order of processing the node pairs. The confidence intervals are negligibly small and are not depicted.

Fig. 5(a) depicts the minimum average EPR pair rates received by any node pair in the simple network topology depicted in Fig. 4 when placing the source at node A and a WSS loss of 8 dB. We can calculate the optimal solution using ILP for this configuration. We note that the $1/(m-k+1)$ approximation algorithm is close to optimal. Modified LPT and First-Fit algorithms perform well; the First-Fit algorithm's performance is surprising given its relative simplicity. Random and round-robin algorithms perform poorly. The $\max(0, T_{\text{f-opt}} - \max_{(i,j),x} \eta_{(i,j)}\bar{n}_x)$ algorithm shows the poorest performance on this metric since it does not assign any channels to some node pairs.

Fig. 5(b) shows the performance of these strategies on the Jain index. The ILP solution, which optimizes for the minimum average received EPR pair rate, also performs the best on this fairness measure. The performance of the other strategies is comparable to each other. Interestingly, despite not assigning any channels to some requests, $\max(0, T_{\text{f-opt}} - \max_{(i,j),x} \eta_{(i,j)}\bar{n}_x)$ strategy performs better on the Jain index than the $1/(m-k+1)$ approximation algorithm. The $1/(m-k+1)$ approximation algorithm, which performed well for minimum photons received, performs the poorest on the Jain index. This underscores a constraint of the Jain index as a metric, as it solely evaluates the relative fairness among assignments without taking into account the quantity of EPR pairs allocated.

Fig. 6(a) shows the normalized and unnormalized minimum average EPR pair rates that any node pair can receive in the ILEC network topology depicted in Fig. 3 when the source is positioned at different locations in the network. These results are for two distinct cases, with WSS losses of 4 dB and 8 dB. Due to the complexity of the ILP program for this topology, we cannot calculate the optimal solution here.

The number of intermediate nodes traversed by a path in the ILEC network varies significantly based on the source node location. A linear increase in the number of intermediate nodes traversed leads to an exponential shift in the associated transmittance of the path. Hence we see that minimum average EPR pair rates vary significantly across source node locations. Also due to this exponential relationship between path loss in dB and transmittance, the difference in the minimum average EPR pair rates across source node locations is accentuated when the WSS loss is set to 8dB as opposed to 4 dB.

Normalized values for the minimum number of EPR pairs facilitate comparisons across diverse network topologies, as in the case of comparison between results in 5(a) and results in 6(a) with an 8 dB loss. However, the reference for normalization is affected when the WSS loss is changed. Decreasing the WSS loss from 8 dB to 4 dB significantly changes the scale of values after normalization, as can be seen in the two sub-graphs in 6(a). This behavior arises because, while the ratio between path losses stays roughly constant when WSS losses are doubled, normalization here captures the ratio between the transmittance of the paths, which has an exponential relationship with dB loss. As a result, highly connected graphs perform better at higher losses, as seen in the figure.

Consistent with the findings displayed for the basic network, both the $1/(m-k+1)$ algorithm and modified LPT algorithms are effective in optimizing the minimum average ERP pair rates received by a node pair. However, the First-Fit algorithm, which

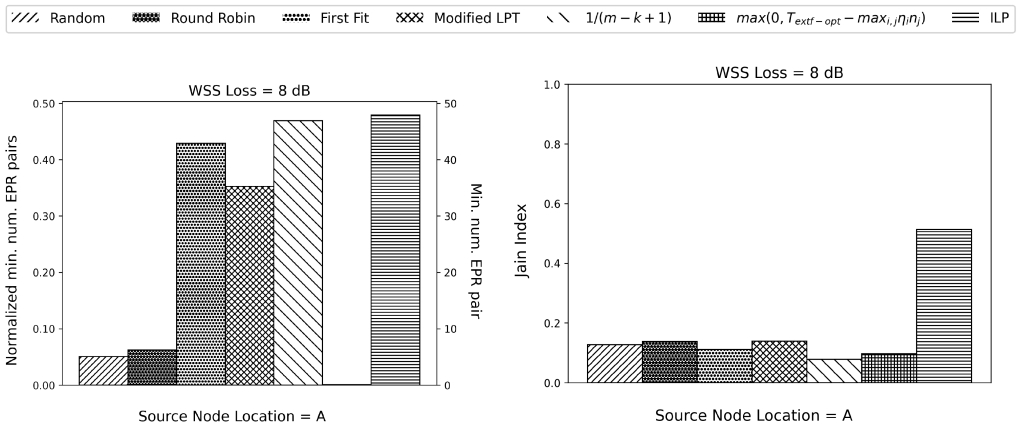

(a) Minimum average received EPR pair rates

(b) Jain Index

Fig. 5. Comparison of performance using different allocation strategies on the simple network depicted in Fig. 4 for 8 dB WSS loss. 5(a) shows normalized (left-axis label) and unnormalized (right-axis label) minimum average EPR pair rates received by any node pair.

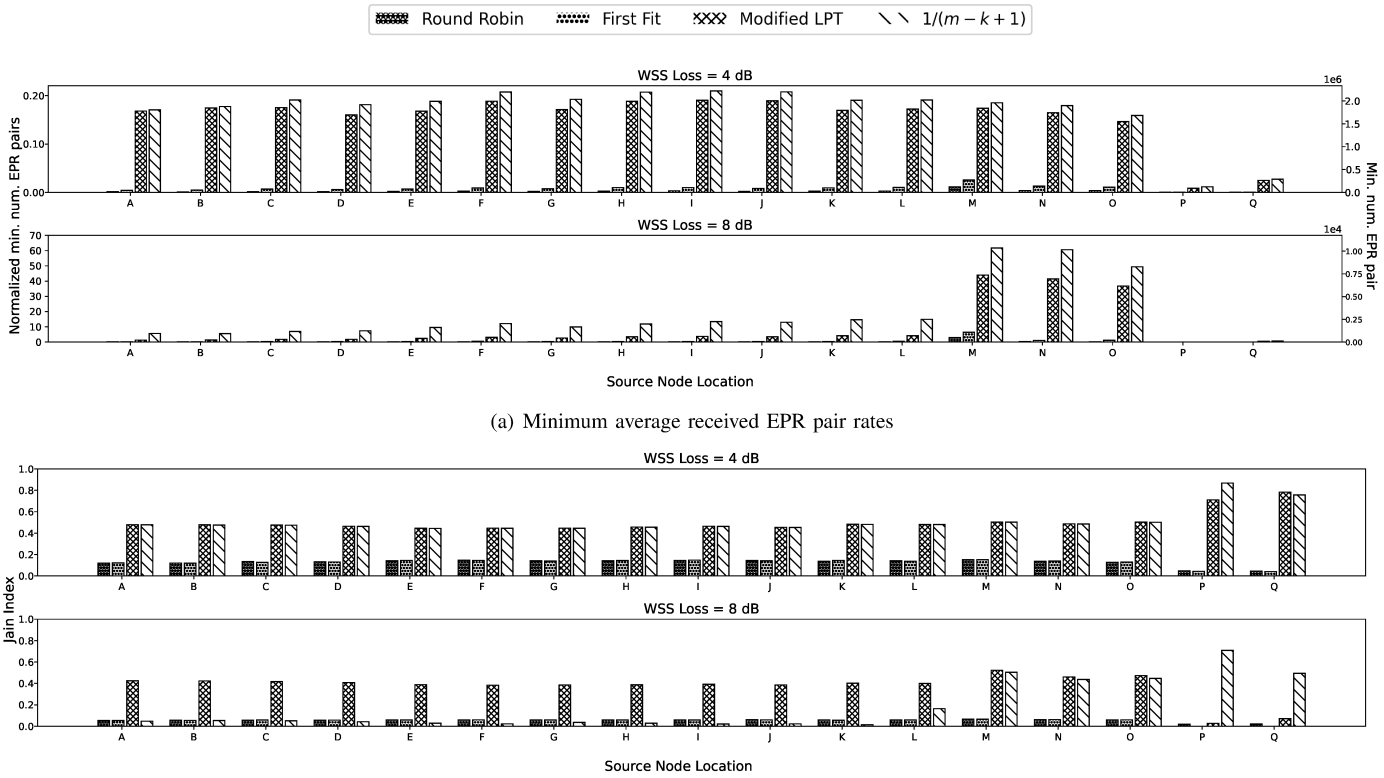

(a) Minimum average received EPR pair rates

(b) Jain index

Fig. 6. Comparison of performance using different allocation strategies on the ILEC network depicted in Fig. 3 for 4 dB and 8 dB WSS loss. 6(a) shows normalized (left-axis label) and unnormalized (right-axis label) minimum average EPR pair rates received by any node pair.

performed well on the simple topology from Fig. 4, performs poorly here. This is due to the greater disparity in the 'value' of a channel to different node pairs in the ILEC network, owing to the greater difference in path losses to these node pairs. For the First-Fit algorithm, situations may arise where no 'high-value' channels are available by the time a node pair with highly lossy paths reaches its turn.

Fig. 6(b) shows the performance of these strategies on the Jain index. The $1/(m-k+1)$ algorithm and LPT strategy both show the best performance on this metric. The $1/(m-k+1)$ strategy

exhibits superior performance compared to other approaches on source nodes P and Q when the WSS loss is at 8 dB.

Across different source locations, we see those with higher nodal degrees can supply higher minimum average EPR rates throughout the network. Nodes A through L have degree 14, and show a similar performance. Node M has the highest degree (16) and shows the best performance. Nodes P and Q have degree two and four, respectively, and demonstrate the poorest performance. Interestingly, the performance of nodes N and O which have degree 15 show dramatic improvement over nodes with degree 14. This can be attributed to the fact that these node's neighbours are neighbors to node Q and second-order neighbors to node P; two nodes that have few other neighbors. Thus while the nodes with 14 neighbors cannot efficiently supply EPR pairs when one of the nodes is P or Q, source nodes N and O do not suffer from this problem.

V. Conclusion

In this study, we explore the optimization of EPR pair distribution in quantum networks to address the increasing demand for efficient quantum computation and communication. We consider a source-in-the-middle time-frequency-heralded architecture and examine optimal routing and various approaches for fair spectrum allocation that approximate the optimal NP-hard solution. For the latter, we find that the $1/(m-k+1)$ approximation and modified LPT algorithms outperform others in EPR pair rate while being comparable to others in fairness as measured by the Jain index. Future work should focus on algorithm refinement and experimental implementations.

Acknowledgment

This material is based upon work supported by the National Science Foundation under Grant No. CNS-2107265 and Science Foundation Ireland grants 20/US/3708, 21/US-C2C/3750, and 13/RC/2077_P2.

We thank Vikash Kumar, Vivek Vasan, Dmitrii Briantcev, Prajit Dhara, Kevin C. Chen, Gabe Richardson, Dennis McNulty, and Robert Norwood for useful discussions on this work.

References

[1] A. Singh, K. Dev, H. Siljak, H. D. Joshi, and M. Magarini, "Quantum Internet—Applications, Functionalities, Enabling Technologies, Challenges, and Research Directions", IEEE Commun. Surveys Tutor., vol. 23, no. 4, pp. 2218–2247, 2021.

[2] K. C. Chen et al., "Zero-Added-Loss Entangled Photon Multiplexing for Ground- and Space-Based Quantum Networks," Phys. Rev. Appl, vol. 19, no. 5, p. 054029, May 2023.

[3] J. M. Simmons, Optical Network Design and Planning. Cham Springer International Publishing, 2014.

[4] J. W. Suurballe and R. E. Tarjan, "A quick method for finding shortest pairs of disjoint paths," Networks, vol. 14, no. 2, pp. 325–336, 1984.

[5] S. Banerjee, R. K. Ghosh, and A. P. K. Reddy, "Parallel Algorithm for Shortest Pairs of Edge-Disjoint Paths", J. Parallel Distrib. Comput., vol. 33, no. 2, pp. 165–171, 1996.

[6] B. C. Chatterjee, N. Sarma, and E. Oki, "Routing and Spectrum Allocation in Elastic Optical Networks: A Tutorial," IEEE Commun. Surv. Tutor., vol. 17, no. 3, pp. 1776–1800, 2015.

[7] W. Chen et al., "Field experiment on a 'star type' metropolitan quantum key distribution network," IEEE Photon. Technol. Lett., vol. 21, no. 9, pp. 575–577, May 1, 2009

[8] S. Wengerowsky, S. K. Joshi, F. Steinlechner, H. Hübel, and R. Ursin, "An entanglement-based wavelength-multiplexed quantum communication network", Nature, vol. 564, no. 7735, pp. 225–228, Dec. 2018.

[9] E. Y. Zhu, C. Corbari, A. Gladyshev, P. G. Kazansky, H.-K. Lo, and L. Qian, "Toward a reconfigurable quantum network enabled by a broadband entangled source", J. Opt. Soc. Am. B, vol. 36, no. 3, pp. B1–B6, Mar. 2019.

[10] R. Wang et al., "A Dynamic Multi-Protocol Entanglement Distribution Quantum Network", in Proc. Opt. Fiber Commun. Conf. Exhib. (OFC), 2022.

[11] M. J. Clark, et al., "Polarisation Based Entanglement Distribution Quantum Networking," MIPRO, Opatija, Croatia: IEEE, May 2023, pp. 271–274.

[12] Lumentum Holdings Inc, "TrueFlex® Twin High Port Count Wavelength Selective Switch (Twin WSS)" datasheet, Nov. 1997 [Revised Sept. 2002].

[13] P. D. Colbourne, S. McLaughlin, C. Murley, S. Gaudet and D. Burke, "Contentionless Twin 8×24 WSS with Low Insertion Loss," Proc. Opt. Fiber Commun. Conf. Exhib. (OFC), San Diego, CA, USA, 2018, pp. 1-3.

[14] J. Yu, Y. Li, M. Bhopalwala, S. Das, M. Ruffini and D. C. Kilper, "Midhaul transmission using edge data centers with split PHY processing and wavelength reassignment for 5G wireless networks," 2018 International Conference on Optical Network Design and Modeling (ONDM), Dublin, Ireland, 2018, pp. 178-183.

[15] Y. Li et al., "Joint Optimization of BBU Pool Allocation and Selection for C-RAN Networks," OFC, San Diego, California: OSA, 2018, p. Th1B.5.

[16] "Optical Loss & Testing Overview — Kingfisher International." Accessed: Oct. 11, 2023. [Online]. Available: https://kingfisherfiber.com/application-notes/optical-loss-testing-overview/

[17] I. Bezáková and V. Dani, "Allocating indivisible goods," SIGecom Exch., vol. 5, no. 3, pp. 11–18, Apr. 2005.

[18] H. Aziz, I. Caragiannis, A. Igarashi, and T. Walsh, "Fair allocation of indivisible goods and chores," Auton. Agents Multi-Agent Syst. vol. 36, no. 1, p. 3, Apr. 2022.

[19] R. L. Graham, "Bounds on Multiprocessing Timing Anomalies," SIAM J. Appl. Math., vol. 17, no. 2, pp. 416–429, 1969.

[20] B. L. Deuermeyer, D. K. Friesen, and M. A. Langston, "Scheduling to Maximize the Minimum Processor Finish Time in a Multiprocessor System," SIAM. J. Alg. Disc. Meth., vol. 3, no. 2, pp. 190–196, Jun. 1982.

[21] B. Y. Wu, "An analysis of the LPT algorithm for the max–min and the min–ratio partition problems", Theor. Comput. Sci., vol. 349, no. 3, pp. 407–419, 2005.

[22] R. K. Jain, D.-M. W. Chiu, and W. R. Hawe, "A quantitative measurement of fairness and discrimination for resource allocation in shared computer system," Eastern Research Laboratory, Digital Equipment Corporation: Hudson, MA, USA, vol. 2, 1984.